

This is the **accepted version** of the article:

Díaz, Raquel; Pallarès, Victor; Cano Garrido, Olivia; [et al.]. «Selective CXCR4+ Cancer Cell Targeting and Potent Antineoplastic Effect by a Nanostructured Version of Recombinant Ricin». *Small*, Vol. 14, issue 26 (June 2018), art. 1800665. DOI 10.1002/sml.201800665

This version is available at <https://ddd.uab.cat/record/236681>

under the terms of the  ^{IN} COPYRIGHT license

DOI: 10.1002/ ((please add manuscript number))

Article type: Full paper

Selective CXCR4⁺ cancer cell targeting and potent antineoplastic effect by a nanostructured version of recombinant ricin

Raquel Díaz^{1, 2, 3 §}, *Dr Victor Pallarès*^{4 §}, *Dr Olivia Cano-Garrido*^{1, 2, 3}, *Naroa Serna*^{1, 2, 3}, *Laura Sánchez-García*^{1, 2, 3}, *Aida Falgàs*^{3, 4}, *Dr Mireia Pesarrodonà*^{1, 2, 3}, *Dr Ugutz Unzueta*^{3, 4}, *Dr Alejandro Sánchez-Chardi*⁵, *Dr Julieta M. Sánchez*^{1,6}, *Dr Isolda Casanova*^{3,4*}, *Dr Esther Vázquez*^{1, 2, 3}, *Prof Ramón Mangues*^{3,4}, *Prof Antonio Villaverde*^{1, 2, 3*}

¹ Institut de Biotecnologia i de Biomedicina, Universitat Autònoma de Barcelona, Bellaterra, 08193 Barcelona, Spain

² Departament de Genètica i de Microbiologia, Universitat Autònoma de Barcelona, Bellaterra, 08193 Barcelona, Spain

³ CIBER de Bioingeniería, Biomateriales y Nanomedicina (CIBER-BBN), Bellaterra, 08193 Barcelona, Spain

⁴ Biomedical Research Institute Sant Pau (IIB-Sant Pau) and Josep Carreras Research Institute, Hospital de la Santa Creu i Sant Pau, 08025 Barcelona, Spain

⁵ Servei de Microscòpia, Universitat Autònoma de Barcelona, Bellaterra, 08193 Barcelona, Spain

⁶ Instituto de Investigaciones Biológicas y Tecnológicas (IIBYT) (CONICET-Universidad Nacional de Córdoba). ICTA & Cátedra de Química Biológica, Departamento de Química, FCEyN, UNC. Av. Velez Sarsfield 1611, X 5016GCA Córdoba, Argentina

§ Equally contributed

* Corresponding authors IC: ICasanova@santpau.cat; AV: Antoni.Villaverde@uab.cat

Keywords: Protein engineering, self-assembling, nanoparticles, acute myeloid leukemia, targeted drug delivery

Under the unmet need of efficient tumor-targeted drugs for oncology, a recombinant version of the plant toxin ricin (the modular protein T22-mRTA-H6) was engineered to self-assemble as protein-only, CXCR4-targeted nanoparticles. The soluble version of the construct self-organized as regular 11 nm-planar entities that were highly cytotoxic in cultured CXCR4⁺ cancer cells upon short time exposure, with a determined IC₅₀ in the nanomolar order of magnitude. The chemical inhibition of CXCR4 binding sites in exposed cells results in a dramatic reduction of the cytotoxic potency, proving the receptor-dependent mechanism of cytotoxicity. The insoluble version of T22-mRTA-H6 was, contrarily, moderately active, indicating that free, nanostructured protein is the optimal drug form. In animal models of acute myeloid leukemia T22-mRTA-H6 nanoparticles showed an impressive and highly selective therapeutic effect, dramatically reducing the leukemia cells affectation of clinically relevant organs. Functionalized T22-mRTA-H6 nanoparticles are then promising prototypes of chemically homogeneous, highly potent anti-tumor nanostructured toxins for precise oncotherapies based on self-mediated intracellular drug delivery.

1. Introduction

Cancer is a major, growing, and unsolved health problem worldwide, with an incidence of 454.8 new cases per 100,000 (men and women) per year, and a mortality of 207.9 per 100,000 men and 145.4 per 100,000 women (US data; <https://www.cancer.gov/about-cancer/understanding/statistics>). Only in 2018, 1,735,350 new cancer cases and 609,640 cancer deaths are projected to occur in the United States.^[1] Conventional cancer treatments continue to be based on potent small molecular weight chemicals administered systemically. Since these drugs are not targeted to cancer cells they do not preferentially accumulate in tumor or metastasis. Biodistributed across healthy tissues, they promote severe hepatic and renal damage that often results in numerous life-threatening side effects.^[2] In the line with the

development of new and improved drugs, drug nanoconjugates, therapeutic antibodies, antibody-drug conjugates, tumor-targeted nanoscale vehicles and tumor-targeted toxins (such as immunotoxins) are being designed to gain specificity and potency, with still limited therapeutic improvement. ^[3] The nanoscale size of the drug, potentially reachable by coupling to a vehicle, minimizes renal clearance and favors the enhanced permeability and retention (EPR) effect. ^[4] Among the set of tested new drugs, protein toxins emerge as a very appealing alternative. ^[3] Proteins are biocompatible macromolecules, easily produced by recombinant DNA technologies, and more than 400 protein species have been already approved for use in humans. ^[5] As versatile molecules, they are suitable for fine tuning through protein fusion technologies, to incorporate relevant functions for use as targeted drugs (such as ligands to specific cell surface tumoral markers). ^[6] Engineered versions of natural protein toxins have become promising anti-tumor agents. The *Corynebacterium diphtheriae* toxin fused to interleukin-2 (Denileukin diftitox, ONTAK®), is an FDA-approved drug that targets leukemia and lymphoma cell types that display IL-2 receptors. ^[7] The exotoxin A from *Pseudomonas aeruginosa* has been also produced through recombinant methodologies in different versions (SS1P, LMB-2, or BL22), which are under clinical trials for the treatment of mesothelioma and leukemia. ^[8, 9]

Compared to microbial toxins, plant toxins are extremely potent molecules. ^[3, 10, 11] Many of them (such as ricin, saporin, abrin, trichosanthin, bouganin and gelonin) are ribosome inactivating proteins (RIPs). Being N-glycosidases, they irreversibly depurinate a single adenine residue in the 23S/25S/28S rRNA stem-loop. This action blocks protein translation and leads to fast cell death. Ricin, a RIP originally extracted from the seeds of *Ricinus communis* of approximately 65 kDa, consists in two chains linked by a disulfide bond; the chain A (RTA) with N-glycosidase enzymatic activity and the chain B (RTB) with lectin properties which binds carbohydrate ligands on target cell surface. ^[12] A single ricin molecule

is estimated to inactivate 1,500-2,000 ribosomes per minute, ^[13] being very promising as highly active cytotoxic protein drug. We have previously identified the peptide T22, an efficient ligand of the cell surface marker CXCR4 (a cytokine receptor selectively over-expressed in metastatic cells of many cancer types, ^[14-19]), as a targeting agent for the precise tumor delivery of protein-only self-assembling nanoparticles. ^[20, 21] Some of these constructs have been built by the controlled oligomerization of proteins with cytotoxic activity, such as pro-apoptotic factors, ^[22] anti-cancer peptides ^[22] and microbial toxins. ^[23] In this context, we intended to confer CXCR4⁺ cell-targeted delivery of ricin assembled as protein nanoparticles to determine their selectivity in cell internalization and their performance as cytotoxic drugs. This has been done through *in vivo* administration of either soluble CXCR4-targeted protein nanoparticles formed by ricin as building blocks or to particular protein-releasing amyloid aggregates formed by CXCR4-targeted ricin, named bacterial inclusion bodies (IBs), ^[24] that might represent a steady source of functional protein for advanced therapies. ^[25-27]

2. Results

The recombinant T22-mRTA-H6 (**Figure 1 A**) was successfully produced in *Escherichia coli* Origami B, purified by His-based one-step affinity chromatography and detected as a single protein species with the expected molecular mass of 35.91 kDa (Figure 1 B), that was fully confirmed by mass spectrometry (not shown). The pure protein was straightforwardly observed by both, DLS and FESEM, as ~11 nm entities occurring in the storage buffer without further treatment (Figure 1 C, D), indicating the spontaneous formation of self-assembled nanoparticles. This was the expected outcome as the combination of cationic peptides at the amino terminus and polyhistidines at the carboxy terminus has been proved to be optimal to promote protein oligomerization as regular nanostructures, ^[28] irrespective of the core protein segment (ricin, in the case of T22-mRTA-H6, Figure 1 A). Treating the material with SDS

resulted in monomers of 5.5 nm (Figure 1 C), which represented the probable building blocks of the nanoparticles. In the related self-assembling protein T22-GFP-H6, in which the sizes of the building block and the assembled version are both equivalent to those of T22-mRTA-H6, the use of small-angle X-ray scattering and other sophisticated analytical methods [29] as well as *in silico* modelling [30] have revealed that the nanoparticle was formed by approximately 10 monomers. Being estimative, this figure fits also to T22-mRTA-H6. The analysis of T22-mRTA-H6 nanoparticles by circular dichroism (CD) revealed a structural composition in which α -helix predominates (29.2 %, Figure 1 E). However, a Thioflavin T (Th T) assay has also revealed the occurrence of intermolecular β -sheet interactions (Figure 1 F) that might contribute to the stability of protein nanoparticles, and that is also compatible with the extent of important β -sheet structure found in the CD (Figure 1 E). Since the nanostructured ricin was intended to be delivered in tumoral tissues, we wondered if the nanoparticles could be still stable in the abnormal pH values observed in the tumor environment, that have been reported to range from approximately 6.3 (intracellular) to 7.4 (extracellular). [31, 32] As observed, T22-mRTA-H6 remained fully assembled under these conditions (Figure 1 F), what supports the usability of construct from the stability point of view.

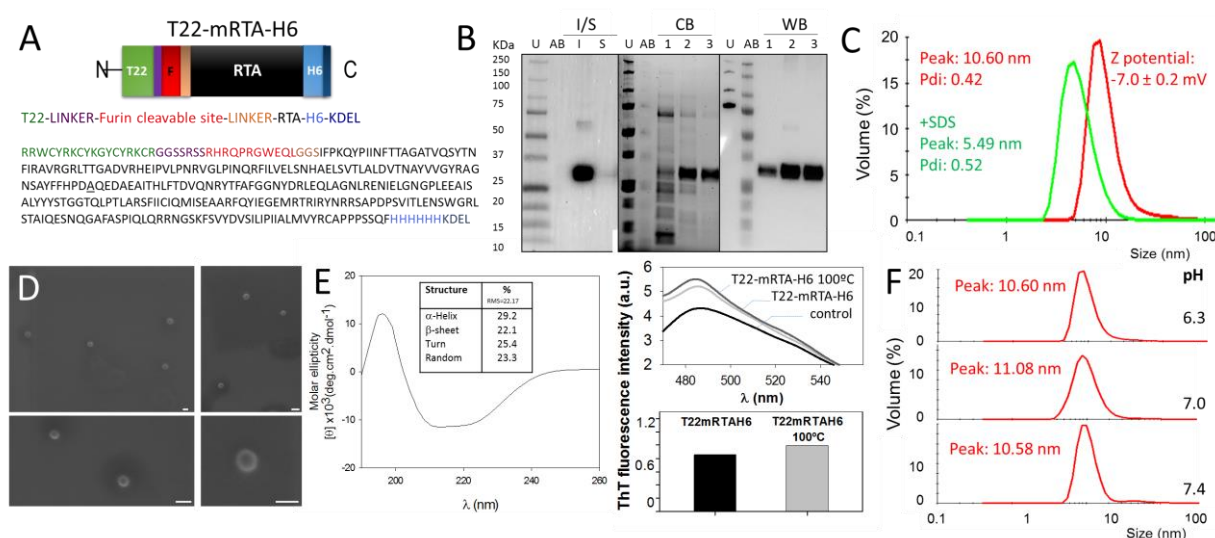


Figure 1. Physicochemical properties of T22-mRTA-H6. A. Modular scheme and amino acid sequence of T22-mRTA-H6. mRTA is the modified fragment A of ricin, described in

material and methods, in which the Asn residue 123 has been replaced by Ala (underlined). Sizes of the boxes are only indicative. B. Fractioning between insoluble (I) and soluble (S) cell fractions in total cell extracts, revealed by WB, upon protein production at 37 °C for 3 h. SDS-PAGE analysis of T22-mRTA-H6 upon one-step affinity purification, revealed by Coomassie blue (CB) staining and by Western blot (WB) using an anti-his antibody. U and AB stand for Unstained and All Blue markers respectively (Bio-Rad, Refs161-0363 and 161-0373), and 1, 2 and 3 indicate, respectively, the unspecific elution peak and two peaks with increasing level of purity. Protein in peak 3 was used in further experiments. C. Hydrodynamic size (and Z potential) of T22-mRTA-H6 nanoparticles formed spontaneously upon purification (red line), determined by DLS. Pdi is polydispersion index, and all figures indicate nm. The size of the monomer, determined upon disassembling the material with 1 % SDS for 40 min, is also indicated (green line). D. FESEM imaging, at different magnifications, of T22-mRTA-H6 nanoparticles. Bars represent 20 nm. E. Far UV CD of T22-mRTA-H6 in carbonate-bicarbonate buffer at pH 8 measured at 25°C. F. ThT fluorescence emission spectra alone (black line) or in the presence of T22-mRTA-H6 (light grey line) and T22-mRTA-H6 previously heated at 100°C (dark grey line). $\lambda_{ex}=450$ nm. In the plot at the bottom, ThT fluorescence emission at 490 nm of T22-mRTA-H6 (black bar) and T22-mRTA-H6 previously heated at 100°C (grey bars). G. Size of T22-mRTA-H6 nanoparticles dialyzed against 51 mM sodium phosphate, 158.6 mM trehalose dehydrate, 0.01 % polysorbate-20 buffer at different pH values, determined by DLS.

In order to test the functionality of the recombinant ricin in such assembled form, cultured CXCR4⁺ HeLa cells were exposed to different concentrations of ricin-based nanoparticles. These materials showed a potent, dose-dependent cytotoxicity that essentially abolished cell viability at 100 nM (**Figure 2 A**). After 72 h of exposure, the IC₅₀ was determined to be 13 ± 0.5 nM. To confirm if, as expected, T22-mRTA-H6-mediated cell death was dependent on its cell binding and internalization of the protein via the cell surface receptor CXCR4 and its ligand T22, we tested if a potent CXCR4 antagonist, AMD3100, ^[33] could be able to recover cell viability when used as a competitor of the toxin, at a molar ratio of 10:1. As observed (**Figure 2 B**), AMD3100 dramatically enhanced cell viability in T22-mRTA-H6-treated cells proving a specific, receptor-mediated penetration of the nanoparticles into target cells. To further confirm such precision cell entry mechanism, we decided to expose non tumoral (CXCR4⁻) 3T3 cells and representative CXCR4⁻ and CXCR4⁺ tumoral cell lines to T22-mRTA-H6, and also to a conventional chemical drug used in the treatment of several cancer types but specially of acute myeloid leukemia (AML), namely cytosine arabinoside (Ara-C).

[34] These cell lines, with different levels of CXCR4 expression (Figure 2 C), supported different levels of protein internalization mediated by the specific interaction between T22 and CXCR4 (Figure 2 D). This was determined through the uptake of T22-GFP-H6, a self-assembling fluorescent protein closely related to T22-mRTA-H6, that contains the same ligand of CXCR4 also accommodated at the amino terminus of the polypeptide. [28] It must be noted that as predicted, CXCR4 expression and T22-mediated protein internalization showed a parallel behavior (compare Figure 2 C and D). Then, when they were finally comparatively tested, the ricin-based protein nanoparticle promoted specific cell death only in CXCR4⁺ cancer cells but not in normal cells, at a dose (100 nM) at which Ara-C did not show any toxic effect on any of these cell lines (Figure 2 E). This observation proved not only the effective targeting of the protein drug but also its superior cytotoxicity compared to an equimolar dose of the model chemical drug.

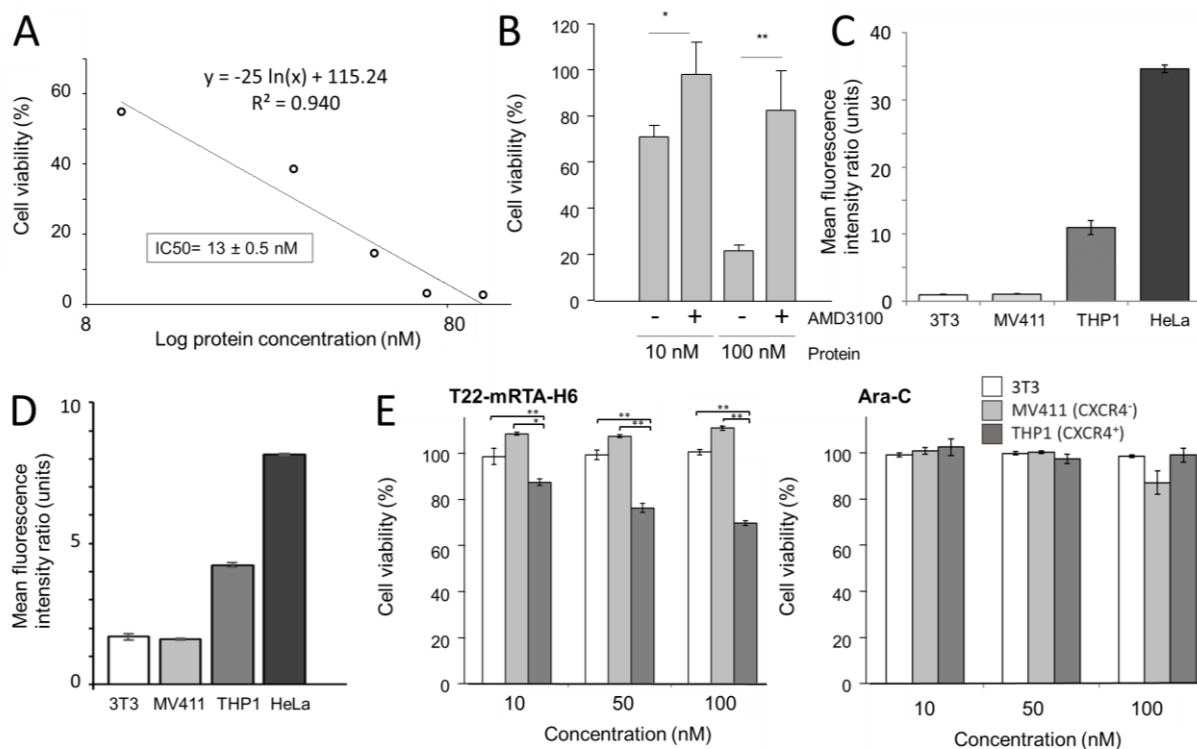


Figure 2. Cytotoxicity and CXCR4 specificity of T22-mRTA-H6 nanoparticles. A. Viability of cultured CXCR4⁺ HeLa cells upon 72 h of exposure to T22-mRTA-H6 nanoparticles at different concentrations, presented as a dose-response curve. B. Inhibition of

cell death in HeLa cells exposed to different concentrations of T22-mRTA-H6 nanoparticles for 72 h, mediated by the CXCR4 antagonist AMD3100 (always at an excess molar ratio of 10:1). C. Levels of CXCR4 membrane protein determined by flow cytometry of different cell lines (3T3, MV411, THP1 and HeLa), expressed as mean fluorescence intensity ratio \pm SE. D. Extent of internalization of 100 nM T22-GFP-H6 in the different cell lines at 1 h of exposure. Results are expressed as mean fluorescence intensity ratio \pm SE. E. Viability of cultured CXCR4⁻ 3T3 cells upon 48 h of exposure to T22-mRTA-H6 nanoparticles and the small molecular weight antitumoral drug Ara-C, at different concentrations. The commercial CXCR4⁻ and CXCR4⁺ human AML cell lines (MV411 and THP1 respectively) are included as controls. Ara-C showed cytotoxicity above 100 nM (not shown). The standard error is represented in all bars. The level of significance is indicated by superscripts (* $p < 0.05$, ** $p < 0.01$).

At this stage, we wanted to confirm that the cytotoxicity promoted by T22-mRTA-H6 was linked to the uptake of the nanoparticles inside CXCR4⁺ cells, and triggered from within. This was reached by exposing HeLa cells to ATTO-labelled nanoparticles and monitoring internalization. As observed (**Figure 3 A**), nanoparticles were internalized by cells at least up to 24 h. As expected for an active version of ricin, apoptosis was detected through both annexin affinity assay and by Hoechst staining (Figure 3 B), and the number of apoptotic cells seemed to peak at around 15-24 h post exposure. In addition, mitochondrial damage was confirmed by the significant increase in the number of cells with lowered JC-1 red fluorescence at 15 and 24 h after treatment with T22-mRTA-H6 (Figure 3 C), indicative of a depolarization in the mitochondrial $\Delta\Psi$ linked to apoptotic induction. Interestingly, cell damage occurred without a detectable increase in reactive oxygen species (ROS, Figure 3 D), while the formation of apoptotic bodies in ricin-exposed HeLa cells was clearly caspase-dependent (Figure 3 E). The combination of these data indicates that T22-mRTA-H6-mediated cell death occurs by a classical caspase-dependent apoptosis pathway.

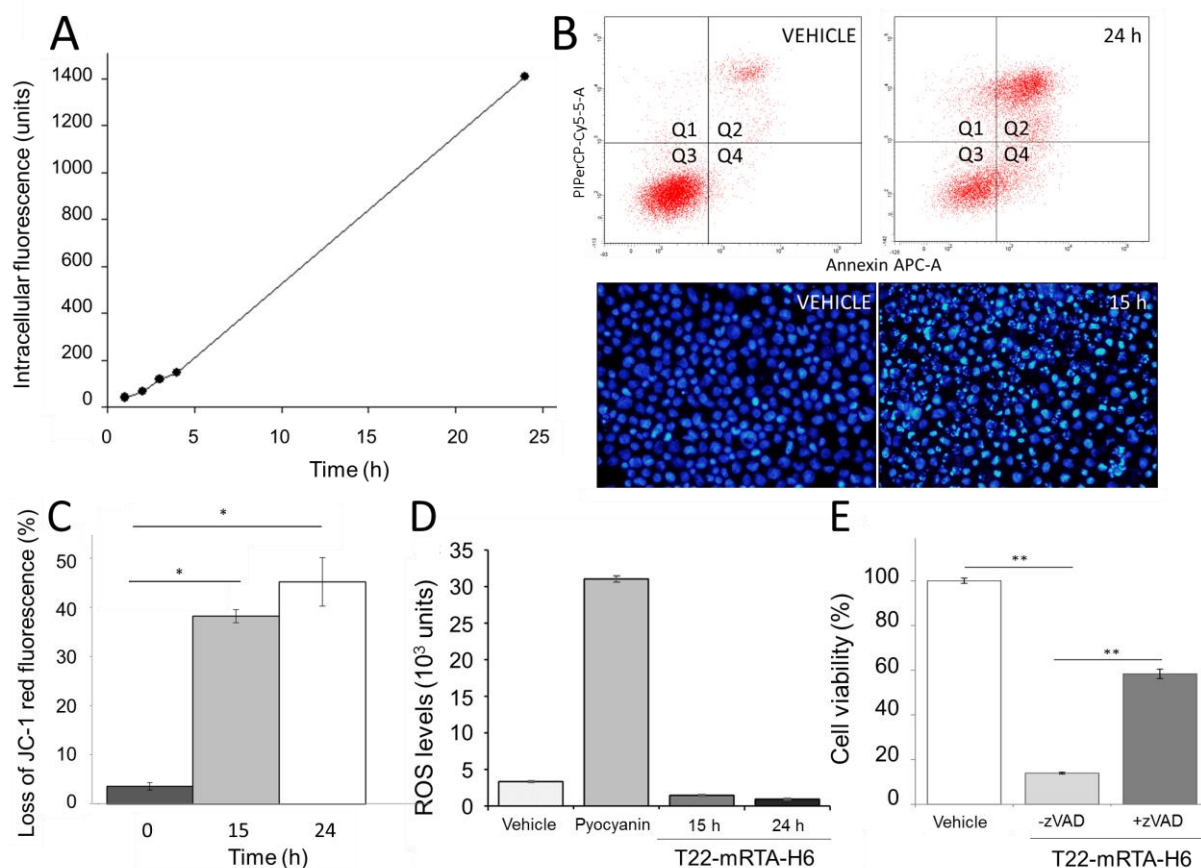


Figure 3. Cell penetrability and intracellular toxicity of T22-mRTA-H6 nanoparticles. A. Intracellular fluorescence in cultured HeLa cells exposed to 100 nM of ATTO488 stained T22-mRTA-H6. Extracellular fluorescence was fully removed by a hash trypsin treatment as described [35]. B. Under the same conditions, the externalized phosphatidylserine was detected by Annexin V Detection Kit (APC, eBioscience) in cells exposed to non-stained T22-mRTA-H6. Dead cells were spotted with propidium iodide (PI). Quadrant Q1 shows HeLa cells marked with PI. Q2 shows cells marked with Annexin V and PI. Q3 shows cells without PI nor Annexin V. Q4 shows cells marked with Annexin V. Therefore, dead cells are shown in Q1 and Q2 while living cells in Q3 and Q4. Apoptotic cells are shown in Q4. At the bottom, Hoechst staining of HeLa cell under the above conditions. Images were obtained by fluorescence microscopy (x400). C. Loss of JC-1 Red fluorescence in T22-mRTA-H6-treated cells as described above, indicative of a change in the mitochondrial $\Delta\psi$. D. Levels of cellular ROS detected with a fluorescence microplate assay. HeLa cells were treated with either buffer, T22-mRTA-H6 (100 nM, for 15 or 24 hours) or 100 μ M Pyocyanin (1 hour) as a positive control. Values are expressed as relative fluorescence units \pm SE. E. Inhibition of caspases with zVAD-fmk reverses the antitumor activity of T22-mRTA-H6 in HeLa cells. Cells were pretreated for 1 hour with 100 μ M zVAD-fmk and then exposed to 100 nM T22-mRTA-H6 for 48 hours. Cell viability is expressed as the percentage of cell survival compared with the control. Values are mean \pm SE. *Vehicle* indicates treatment with buffer. The level of significance is indicated (* $p < 0.05$, ** $p < 0.01$).

The suitable cell-targeting of the nanostructured version of ricin conferred by the peptide T22 (Figure 2), and the fact that most of the T22-mRTA-H6 protein was obtained in insoluble form (Figure 1 B), prompted us to evaluate if the insoluble version of ricin might also exhibit cell-targeted cytotoxicity. In this context, we have recently described how the presence of T22 and other cell ligands, in recombinant proteins that form bacterial IBs,^[27] allow an efficient and specific cell penetration of the whole protein clusters. In the same conceptual line, bacterial IBs formed by self-assembling proteins might contain quasi-native forms of nanoparticles or assembling precursors.^[36] IB proteins retain functionalities of the soluble protein version and can be gradually released from the aggregates when exposed to cells [26] or when implanted *in vivo* by local injection.^[25] The ultrastructural morphometry of insoluble version of T22-mRTA-H6 was observed in a nearly native state by FESEM as conventional IBs, namely pseudo-spherical protein clusters with an average diameter size ranging from 400 to 600 nm (**Figure 4 A**).

When exposing HeLa cells to increasing amounts of T22-mRTA-H6 IBs, a mild cytotoxic effect was indeed observed (Figure 4 B), although the differences in cell viability, when comparing with untreated cell cultures, were in the limits of significance. In addition, the insoluble version of T22-GFP-H6 (forming similar IBs,^[27]), a self-assembling CXCR4-targeted protein devoid of any cytotoxic domain, also promoted a transient and mild reduction of cell viability. However, in this case, cells showed an immediate recovery at longer time exposures that, in contrast, was not found associated to T22-mRTA-H6. Despite previous data about the potential of functional protein release from IBs,^[25] the biological effect of T22-mRTA-H6 IBs was, in our hands, only moderate.

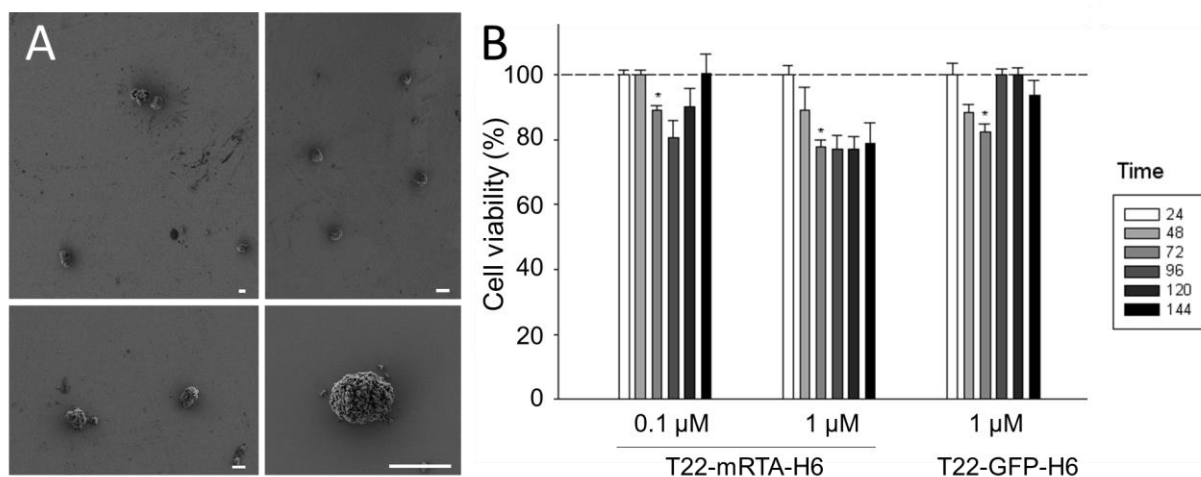


Figure 4. Properties of T22-mRTA-H6 IBs. A. FESEM images of isolated T22-mRTA-H6 IBs at different magnifications. Bars indicate 1 μm. B. Viability of cultured CXCR4⁺ HeLa cells upon different times of exposure to T22-mRTA-H6 IBs and to control, non-functional IBs formed by the related protein T22-GFP-H6. Exposure time is indicated in hours. The standard error is represented by a black line. The level of significance is indicated by superscripts (* p<0.05).

The antitumor effect of both T22-mRTA-H6 soluble nanoparticles and T22-mRTA-H6 IBs was evaluated in a disseminated AML animal model. NSG mice were injected with THP1-Luci cells to generate leukemia dissemination in mice. Two days after cell injection through the vein tail, we performed a single dose injection in the mice hypodermis (SC) of 1 mg of T22-mRTA-H6 IBs in two mice (IB-T22mRTA group). In a different mouse group, we started daily intravenous administrations of 10 μg of soluble T22-mRTA-H6 (T22mRTA group) to one mouse or buffer alone (VEHICLE group) to three mice, for a total of 10 doses. No effects on mice weight were observed during the treatments (data not shown). The progression and dissemination of leukemia was assessed by monitoring BLI using the IVIS Spectrum. From the day 6 and until the end of the experiment, the mouse treated with soluble T22-mRTA-H6 (T22mRTA) showed lower luminescence emission than the VEHICLE group (**Figure 5A**). Thus, as measured by BLI, treatment with soluble T22-mRTA-H6 inhibited the dissemination of AML cells in mice, compared to the vehicle group, after the 4th, 6th, 8th and

10th doses of T22-mRTA-H6 at 10 µg per dose (which corresponded to day 6, 8, 10 or 13 after injection of cells, respectively). In contrast, no differences in BLI were found between mice treated with T22-mRTA-H6 IBs (IB-T22mRTA) and the control VEHICLE mice (Figure 5A).

In a next step, the antitumor activity of nanoparticles was analyzed in affected organs *ex vivo* 14 days after the injection of cells when mice presented signs of advanced disease. The analyses with the IVIS Spectrum showed that the treatment with soluble T22-mRTA-H6 nanoparticles (T22mRTA) decreased BLI in the bone marrow (backbone and hindlimbs), liver and spleen, in contrast to the findings in mice treated with buffer alone (VEHICLE) (Figure 5B). However, the treatment with T22-mRTA-H6 IBs (IB-T22mRTA) did not show changes in BLI in the same tissues in comparison to control mice (VEHICLE) (Figure 5B).

In addition, we evaluated the dissemination of leukemic cells in the affected organs of the animal by IHC of CD45, a human leukocyte marker that detects AML THP1 cells. Results correlated with BLI analyses showing that treatment with soluble T22-mRTA-H6, differently from those registered after T22-mRTA-H6 IBs treatment, reduced the dissemination in the infiltrated tissues, by detecting lower number of CD45 positive cells in bone marrow, liver and spleen in the mouse treated with soluble T22-mRTA-H6 (Figure 5C). Finally, we performed H&E staining of the infiltrated organs and additional organs not affected by leukemia cells. We did not observe any sign of toxicity in any of the affected or unaffected tissues, neither with the soluble T22-mRTA-H6 nor with the T22-mRTA-H6 IBs treatments (Figure 6). As it occurred *in vitro*, IBs caused, if any, just a mild biological effect.

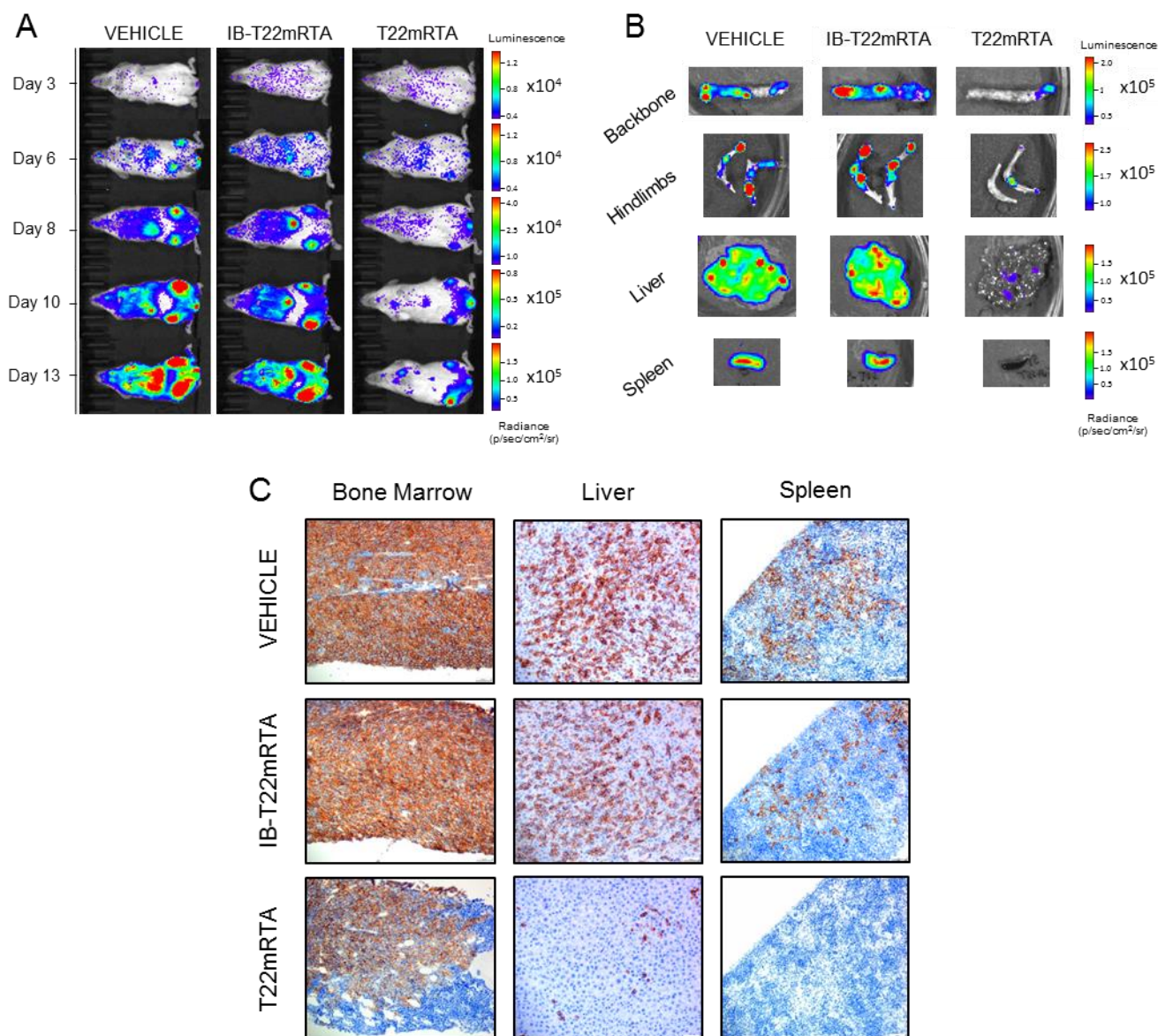


Figure 5. Antitumor activity of T22-mRTA-H6 in a disseminated AML mouse model. A. Follow-up of bioluminescence emitted by mice treated with soluble T22-mRTA-H6 nanoparticles (T22mRTA), T22-mRTA-H6 IBs (IB-T22mRTA) or buffer (VEHICLE) during the 14 days of the experiment, analyzed by IVIS Spectrum. B. Levels of luminescence detected *ex vivo* in IVIS Spectrum in the tissues infiltrated with leukemic cells such as backbone, hindlimbs, liver and spleen of mice treated with buffer (VEHICLE), T22-mRTA-H6 IB (IB-T22mRTA) or soluble T22-mRTA-H6 (T22mRTA). C. Detection of CD45 positive cells by IHQ in spleen, liver and bone marrow of mice treated with buffer (VEHICLE), T22-mRTA-H6 IBs (IB-T22mRTA) or soluble T22-mRTA-H6 nanoparticles (T22mRTA). T22mRTA, mouse treated with soluble T22-mRTA-H6; IB-T22mRTA, mouse group treated with T22-mRTA-H6 IBs; VEHICLE, group treated with vehicle. Bars indicate 50 μ m.

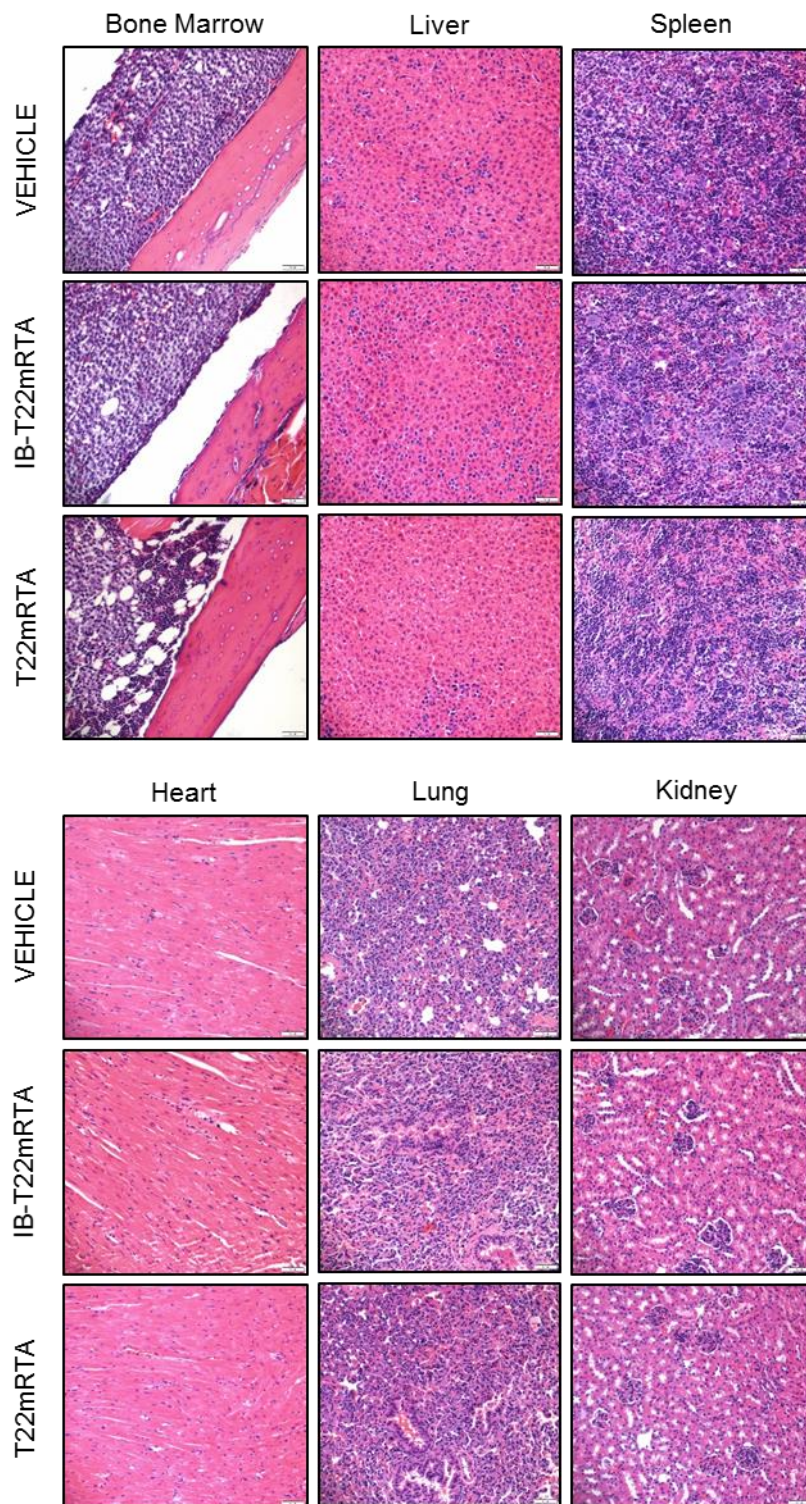


Figure 6. Histopathology in the disseminated AML mouse model after a treatment with T22-mRTA-H6. Hematoxylin and eosin staining of normal (heart, lung, kidney) and leukemia infiltrated organs (bone marrow, liver, spleen). Images were taken in the microscope with a 20x objective and an Olympus DP72 digital camera. H&E, Hematoxylin and Eosin; T22mRTA, mouse treated with soluble T22-mRTA-H6; IB-T22mRTA, mouse group treated with T22-mRTA-H6 IBs; VEHICLE, mouse group treated with buffer. Bars indicate 50 µm.

3. Discussion

Functional recruitment in single chain modular polypeptides is a promising strategy for the generation of self-targeted and self-delivered drugs, that are chemically homogenous and produced in a single step in recombinant cell factories.^[37] Protein drugs represent a big sector in the pharmacological market.^[5] Their easy industrial biofabrication and scalability combined with the intrinsic biocompatibility and functional versatility, approachable by genetic engineering, make proteins a very convenient category of tuneable pharmaceuticals.^[38, 39] In oncology, cytotoxic proteins selected from nature have been engineered and adapted to act as anti-tumor agents, by means of different approaches that must necessarily consider cell targeting.^[3] Immunotoxins are relevant representatives of how protein toxins can be targeted by simple fusion technologies in monovalent complexes, with relevant potential for precise cell killing.^[40-42] However, proper targeting is not regularly achieved in current nanomedicine^[43] and the amount of cell targeted drugs that reach the intended tumor tissues, especially in oncology, is rather limited (usually < 1%).^[44] Specifically, immunotoxins have not so far fulfilled the requirements regarding a convenient therapeutic index, as side toxicity is still relevant.^[3] The combination of highly potent toxins with effective targeting is then necessary for a highly precise and selective cell killing, that might be still optimized by a regular and multivalent display of the targeting agent on the surface of the drug.^[45] Also, formulating a protein drug within the nanoscale size should favor the enhanced permeability and retention effects,^[4] minimizing the biological barriers in the drug delivery process.

Under these premises, we have engineered the highly potent plant toxin ricin as a CXCR4-targeted, protein-only nanoscale drug with a multivalent presentation of the ligand, the peptide T22, reached through the regular self-assembling of ricin as stable 11 nm-nanoparticles (Figure 1 D, F). A related modular protein, namely T22-GFP-H6, that self-

assembles as 12 nm-nanoparticles, has been modelled as oligomerizing in approximately 10 subunits accommodated in a toroid architecture, thus ensuring a sufficient multivalent display of the ligand. ^[29, 30] According to the similarities in the molecular mass of the building block and in the final size of the resulting nanoparticles, T22-mRTA-H6 seems to self-arrange in a similar pattern (Figure 1). Ricin has been largely considered as a drug component in cancer therapies, ^[46] and previously explored in form of immunotoxins with moderate efficacy. ^[47-49] In the nanoconstruct generated here, ricin is highly active and fully potent on target cells, indicative of that oligomerization is not preventing functionality.

This particular approach highly increases the selectivity of the cytotoxic potential of ricin against CXCR4⁺ cancer cells because of the combination of three main and critical effects. Firstly, the specific uptake of the therapeutic protein was achieved because of the multivalent display of the CXCR4 ligand, T22, on the nanoparticle and exclusive CXCR4 receptor overexpression in the target cancer cell membranes. This fact prevents internalization and toxicity on normal cells with low or negligible levels of CXCR4. Secondly, the avoidance of the severe side effects that appeared on previous clinical trials testing ricin anticancer effect that led to their discontinuation. ^[13, 46] Specifically, we incorporated the mutant (N132A) ricin A chain as functional building block of the nanoparticle, to suppress the potential vascular leak syndrome. We also excluded the use of ricin B-chain to block the severe toxicity associated with its non-specific binding to glycoproteins or mannose receptors expressed on the membrane of non-tumor cells (e.g. Kupffer cells of the liver sinusoids). Finally, the enhanced delivery of the biologically active ricin A chain to the cytosol of target cells (Figure 3 A) was reached because of the addition of the furin cleavage site that releases the active domain from the nanoparticle in the endoplasmic reticulum, and a KDEL sequence which allows the translocation of the biologically active toxin to the cytosol, avoiding its lysosomal degradation. The endosomal delivery of the protein drug would also prevent the development

of multidrug resistance, that mainly relates to drug efflux by cancer cells through the ATP-binding cassette (ABC) transporters activity, overexpression of ABC transporters associating with poor response to therapy.^[50] Low molecular weight drugs enter cells by diffusion across membranes, which renders them vulnerable to their efflux by ABC transporters. In contrast, the nanoscale size of oligomeric ricin is expected to avoid passive diffusion. Entering CXCR4⁺ cells through endocytic vesicles, the protein achieves high intracellular concentration in absence of (or reversing) the multidrug resistance phenotype that might have been observed for a free small drug. This effect, associated with the entry route, has been reported for doxorubicin-loaded polymeric nanoparticles and doxorubicin-polymer conjugates, among others.^[51-52]

The combination of these three crucial effects in basic cellular pathways makes for a dramatic increase of ricin A antineoplastic activity. Thus, the previously reported IC₅₀ of untargeted ricin A in HeLa cells (IC₅₀ 36 µg/ml (1 µM))^[53] is here reduced about 100 fold (IC₅₀=13 nM) because of selective CXCR4 cancer cell targeting, KDEL sequence and furin site incorporation into the nanoparticle. The reached IC₅₀ (Figure 2) is in the same nM range than that described by other highly lethal toxins (such as diphtheria toxin derivatives,^[54-56] *Pseudomonas* exotoxin^[57] or neurotoxins^[58]). However, this engineered version is highly promising for the further development of the present prototype as an efficient oncological nanostructured drug, since it keeps the full selectivity for the cell surface cytokine receptor CXCR4 (Figure 2) while keeping a nanostructured organization with a multivalent presentation of the surface receptor (Figure 1). In addition, in a molar basis, T22-mRTA-H6 is more cytotoxic on AML CXCR4⁺ cells than Ara-C (Figure 2 E), a basic chemical drug included in most AML treatment protocols.^[34] Importantly, the precise cytotoxic activity of T22-mRTA-H6 nanoparticles is conserved *in vivo* after systemic administration, which leads to a dramatic blockade of leukemic cell affectation in the clinically relevant organs (bone

marrow, liver and spleen) in the CXCR4⁺ AML model (Figure 5). These findings were associated with absence of any detectable systemic (not shown) or histological toxicity in off-target organs during the experiment time (Figure 6). It could not be fully excluded that in longer treatments ricin (as well as other recombinant toxins or therapeutic fusion proteins) may induce an immune response, that if involving antigens shared with endogenous protein might lead to adverse effects. ^[59, 60] However, the modified version of ricin used here avoids the vascular leak syndrome (VLS), the major concern in the clinical trial of a ricin A-antibody (CD19/CD12) immunotoxin (<https://clinicaltrials.gov/ct2/show/NCT01408160>). In this context, further de-immunization might be feasible, if required, to improve the clinical performance of T22-mRTA-H6 or derived drugs, ensuring low immunogenicity and avoidance of autoimmune diseases. This could be done by an approach similar to that carried out for diphtheria and *Pseudomonas aeruginosa* toxins. These microbial proteins, components of most of third generation immunotoxins under clinical evaluation, are successfully engineered by the removal of non-essential sequences and by the genetic elimination of antigenic T and B cell epitopes, without compromising their antitumor activity. ^[60]

Combining the impressive therapeutic effects observed *in vivo* and the fact that CXCR4 is a tumoral marker relevant in more than 20 human neoplasias, ^[61] its overexpression correlating with aggressiveness, ^[62-66] T22-mRTA-H6 nanoparticles combine selectivity, cytotoxicity, nanoscale size and multivalent display in a chemically homogeneous entity devoid of any external carrier or vehicle that might impose limitations to the biocompatibility of the whole construct. ^[4]

4. Conclusion

One of the most potent toxins in nature, ricin, has been genetically instructed to self-assemble as stable 11 nm-homomeric nanoparticles and to selectively kill CXCR4-overexpressing cells,

by using a promising protein engineering toolkit. The resulting nanoscale material has been shown as highly cytotoxic and highly selective over CXCR4⁺ cells, resulting in an unusually strong and efficient antitumor activity in a mouse model of the difficult-to-treat disseminated acute myeloid leukemia, in complete absence of side-toxicity. This analysis opens a plethora of possibilities to combine highly toxic proteins with a highly selective tumor-targeting platform, that within the nanoscale, would fulfil the emerging concept of self-assembled, self-targeted vehicle-free recombinant drugs for precision medicines.

5. Materials and methods

5.1 Genetic design and protein production

The recombinant protein T22-mRTA-H6 (Figure 1 A) was designed to include the highly specific CXCR4 ligand T22 [20] at the amino terminus followed by a mutated version of the ricin A chain, and a hexahistidine tail at the carboxy terminus. The mutation N132A was introduced to suppress the vascular leak syndrome in potential future *in vivo* administrations, keeping the cytotoxic activity. In addition, a furin cleave site was also incorporated to allow the release of the accessory N-terminal region in the endosome and the intracellular activity of ricin in a quasi-native sequence format. A KDEL motif was also incorporated to favour endosomal escape. [67] The plasmid construct pET22b-T22-mRTA-H6, encoding the protein under the control of the bacteriophage T7 promoter, was generated by GeneArt and transformed into *Escherichia coli* Origami B cells.

5.2 Production and purification of soluble protein

Recombinant bacteria were cultured in lysogeny broth (LB) medium with 100 µg/ml ampicillin, 15 µg/ml kanamycin and 12.5 µg/ml of tetracycline, at 37 °C and 250 rpm. The recombinant gene expression was induced by adding 0.1 mM isopropyl-β-thiogalactopyronaside (IPTG) when the OD of the culture reached a value between 0.5 and 0.7. Cultures were subsequently incubated overnight at 20 °C and 250 rpm. Cells were harvested and centrifuged (5,000 g, 15 min, 4 °C). The cell pellet was resuspended in Wash Buffer (51 mM sodium phosphate buffer, pH=8, 158.6 mM trehalose dihydrate, 0.01%

Polysorbate-20, 15 mM imidazole, 300 mM NaCl) in presence of protease inhibitor cocktail Complete EDTA-Free (Roche). Bacterial cells were sonicated twice at 10% amplitude and once at 15% of amplitude for 10 min each round, centrifuged (15,000 g, 45 min, 4 °C) and soluble fraction purified by affinity chromatography with a HiTrap Chelating HP column in an AKTA purifier FPLC, (GE Healthcare). After the samples were filtered (0.22 µm) and injected into the column, the fractions to be collected were eluted at approximately 30% Elution Buffer (51 mM sodium phosphate, pH=8, 158.6 mM trehalose dihydrate, 0.01% Polysorbate-20, 500 mM imidazole, 300 mM NaCl). The buffer exchange was done in Centricon Centrifugal Tubes Ultracel 10,000 NMWL. T22-mRTA-H6 was found to be highly stable in 51 mM sodium phosphate pH=6.2, 60 mg/ml α-trehalose dehydrate, 0.01% polysorbate-20. Protein purity was analyzed by SDS electrophoresis on TGX Stain-Free gels (Bio-Rad), followed by Western blotting using an anti-His monoclonal antibody (Santa Cruz Biotechnology). Sodium dodecyl sulfate polyacrylamide gel electrophoresis (SDS-PAGE) on TGX Stain-Free Gels (Bio-Rad) was conducted to analyze the protein. Samples were diluted in denaturing buffer (0.53 M Tris Base, 5.52 M glycerol, 0.27 M SDS, 2.84 M β-mercaptoethanol, 7.99 M urea) at a 3:1 molar ratio, boiled at 96°C for 10 min and loaded into the gels lanes. For the Western Blot, an anti-His monoclonal antibody was used (Santa Cruz Biotechnology) followed by a goat anti mouse IgG (H+L)-HRP secondary antibody (Ref: 170-6516) conjugate (Bio-Rad, Ref: 170-6516). Images were observed using ChemiDoc Touch Imaging System. Protein production has been partially performed by the ICTS “NANBIOSIS”, more specifically by the Protein Production Platform of CIBER-BBN/ IBB (<http://www.nanbiosis.es/unit/u1-protein-production-platform-ppp/>)

5.3 Production and purification of insoluble protein

Recombinant bacteria were cultured in LB at 37°C and 250 rpm until the OD reached between 0.5 and 0.7, and gene expression was induced by 1 mM IPTG. Then, cells were further incubated to allow gene expression for 3 h at 37 °C and 250 rpm. After sedimentation (5,000 g, 15 min, 4 °C), the pellet was resuspended in 0.22 µm filtered lysis buffer (Tris 1 M pH=8, NaCl 4 M, EDTA 50 mM) in presence of protease inhibitor cocktail Complete EDTA-Free (Roche), the protease inhibitor phenylmethane sulfonyl fluoride (PMSF, 100 mM) and 50 µg lysozyme/ml, followed by an incubation at 37 °C and 250 rpm for 2 h. Cells were disrupted in a French Press (5 rounds at 1,200 psi) and kept at -80 °C overnight. Samples were thawed and treated 0.2 µl Triton X-100/ml cell culture for 1h at room temperature with agitation. Then,

after sedimentation (15,000 g, 15 min, 4 °C), pellets were resuspended in the same volume of filtered lysis buffer. The following reagents were then added to the sample: 1 µl MgSO₄ (1 M)/ml cell culture, 1 µg DNase/ml cell culture. The culture was then incubated for 1 h at 37 °C and 250 rpm agitation. As a sterility assay, LB plates were seeded with 100 µl of culture at 37 °C, overnight, and the suspension of insoluble protein was frozen at -80 °C overnight. The suspension was frozen and thawed daily until no bacterial colonies appeared in the plates. Then, after sedimentation (15,000 g, 15 min, 4 °C), the supernatant was discarded, and each pellet was resuspended in filtered ultrapure water and aliquots were made. Finally, after sedimentation of insoluble material (15,000 g, 15 min, 4 °C), supernatants were discarded and pellets were stored at -80 °C.

5.4 Quantitative protein analysis

Protein purity was analyzed by sodium dodecyl sulphate polyacrylamide gel electrophoresis (SDS-PAGE) on a Chemi Doc Touch Imaging System (Bio-Rad). Briefly, both soluble and insoluble samples were mixed with denaturing buffer (0.53M Tris Base, 5.52 M glycerol, 0.27 M sodium dodecylsulphate (SDS), 2.84 M β-mercaptoethanol, 7.99 M urea) at a ratio 3:1, boiled for 5 or 45 min, respectively, and loaded onto the gels. For the Western Blot, an anti-His monoclonal antibody was used (Santa Cruz Biotechnology) followed by a goat anti mouse IgG (H+L)-HRP secondary antibody conjugate (Bio-Rad). Gels were scanned at high resolution and bands were quantified with Quantity One Software (Bio-Rad) using a known protein standard of soluble recombinant T22-mRTA-H6.

5.5 Quantitative and qualitative analyses of soluble protein

Protein molecular weight was verified by mass spectrometry (MALDI-TOF), and concentration determined by Bradford Assay (Dye Reagent Concentrate Bio-Rad kit). Volume size distribution of protein nanoparticles was determined by Dynamic Light Scattering (DLS). For that, a 50 µl aliquot (stored at -80 °C) was thawed and the volume size distribution of nanoparticles was immediately determined at 633 nm (Zetasizer Nano ZS, Malvern Instruments Limited). Far-UV circular dichroism (CD) was determined at 25 °C in a Jasco J-715 spectropolarimeter to assess the secondary structure of T22-mRTA-H6, which was dissolved at 0.35 mg/ml in 166 mM sodium bicarbonate buffer, pH 8. The CD spectra were obtained in a 1 mm path-length cuvette over a wavelength range of 190-260 nm, at a

scan rate of 50 nm/min, a response of 1 s and a band-width of 1 nm. Six scans were accumulated. The magnitude of secondary structure was analyzed using the JASCO spectramanager analysis software. To investigate potential intermolecular β -sheet structure in the protein nanoparticles, conventional methods for Thioflavin T (ThT) staining were adapted. Briefly, protein aliquots (10 μ l) were added to 90 μ l of 50 μ M (Sigma Aldrich) in phosphate buffered saline (PBS), pH 7,4 and stirred for 1 min. The final protein concentration was 0.17 mg/ml. ThT was excited at 450 nm and the fluorescence emission spectra was recorded in the range of 460 to 565 nm with a Varian Cary Eclipse spectrofluorimeter. The cross- β -sheet structure was monitored by the enhancement of the free dye fluorescence emission.

5.6 Cell culture and determination of cell viability and apoptosis

HeLa cells (ATCC-CCL-2) were cultured at 37 °C in a 5% CO₂ humidified atmosphere in MEM-Alpha media supplemented with 10% fetal calf serum (Gibco Thermo Fisher Scientific (TFS)). They were seeded in an opaque 96-well plate (3x10⁴ cells/well) for 24 h. When insoluble T22-mRTA-H6 was assayed, the media was supplemented with 2% penicillin, 10,000 U/ml streptomycin (Gibco, TFS). The next day soluble T22-mRTA-H6 was added and cells were exposed for 24, 48 and 72 h). Cells were also exposed to insoluble protein version during 24, 48, 72, 96, 120, and 144 h. Cell viability was determined by CellTiterGlo Luminescent Cell Viability Assay (Promega) in a Multilabel Plater Reader Victor3 (Perkin Elmer). For the CXCR4 specificity assay, the CXCR4 antagonist AMD3100 [33] was added at 10:1 molar ratio 1 h before the incorporation of the protein. Antagonist and protein were incubated in a final volume of 10 μ l that were mixed with 90 μ l of culture media. All soluble protein experiments were done in triplicate and insoluble protein with six replicates.

On the other hand, the AML cell lines THP1 (ACC-16) and MV411 (ACC-102), as well as 3T3 mouse fibroblasts (ACC-173), were purchased from DSMZ (Leibniz Institute DSMZ-German Collection of Microorganisms and Cell Cultures, Braunschweig, Germany). THP1 was cultured in RPMI-1640 medium supplemented with 10% FBS, 10 mmol/l L-glutamine 100 U/ml penicillin, 10 mg/ml streptomycin and 0.45 μ g/ml fungizone. (Gibco, TFS). 3T3 cells were cultured with DMEM medium adding the same supplements. Cells were kept at 37°C in a humidified atmosphere of 5% CO₂. Cell viability assays with these cell lines were performed using the XTT Cell Viability Kit II (Roche Diagnostics) and absorbance was read in a spectrophotometer at 490nm (BMG Labtech). The effect of the caspase inhibitor zVAD-fmk was evaluated pretreating for 1 hour cells seeded on 96-well plates (at 100 μ M zVAD-

fmk) and then exposing them to 100 nM T22-mRTA-H6 for 48 hours. The antitumor drug Ara-C (Cytosine β -D-arabinofuranoside hydrochloride) was purchased from Sigma Aldrich. To allow the follow-up of AML in mice, THP1 AML cell line was transfected with a plasmid encoding the luciferase gene that confers bioluminescence that can be non-invasively imaged (BLI) to the cells. Briefly, THP1 cells were harvested in 24-well plates, treated with 0.5 μ g of DNA plasmid and mixed with Lipofectamine LTX and PLUS reagents (A12621, Invitrogen, TFS) in Opti-MEM Reduced Serum Medium (Gibco, TFS) according to the manufacturer's instructions. 48 hours later BLI levels were tested incubating cells with luciferin in an IVIS Spectrum In Vivo Imaging System (PerkinElmer, Waltham, MA, USA). Finally, transfected cells were selected with 1.5 mg/mL geneticin (G418 Sulfate, Gibco, TFS) and BLI was analyzed periodically to check the preservation of the plasmid in cells, called THP1-Luci cells. Internalization of T22-GFP-H6 ^[30] in 3T3, MV411, THP1 and HeLa was determined by Fluorescence-activated cell sorting (FACS Calibur, BD). Cells were exposed for 1 hour to T22-GFP-H6 at 100 nM. Then, cells were washed with PBS and trypsinized (1 mg/ml trypsin, Life Technologies) in order to remove nonspecific binding of nanoparticles to the cell membrane. Finally, levels of intracellular GFP fluorescence were quantified by flow cytometry. Mean fluorescence intensity ratios are given as mean fluorescence intensity of the treated samples divided by the mean fluorescence intensity of the vehicles.

To evaluate cell apoptosis, we performed nuclear staining with the Hoescht 3342 dye (Sigma-Aldrich) in HeLa cells exposed to 100 nM T22-mRTA-H6 or buffer for different times. Once the incubation was finished, the media was collected and centrifuged to obtain the suspended cells. They were rinsed with PBS and centrifuged again. The adhered cells were trypsinized and pulled together with those previously obtained. These cells were fixed (3.7 % p-formaldehyde in PBS, pH 7.4) for 10 min at -20°C, washed with PBS and resuspended in 10 μ l of PBS. Finally, cells were mounted on a slide with ProLong™ Gold Antifade Mountant with DAPI and observed for the appearance of the nuclei under a fluorescence microscope. In addition, externalized phosphatidylserine protein-exposed cells was detected by Annexin V Detection Kit (APC, eBioscience) while dead cells were spotted with propidium iodide (PI), according to supplier instructions. Cell internalization was monitored using ATTO-labelled protein as described elsewhere. ^[23]

5.7 Determination of ROS levels and mitochondrial damage

On the other hand, levels of cellular ROS were measured with the Cellular ROS Detection Assay Kit (Abcam). In brief, HeLa cells were exposed to 100 nM T22-mRTA-H6 (15 or 24 hours) or buffer. Then, cells were washed and incubated with ROS Detection Solution for 1 hour at 37°C, in the dark, adding 100 µM Pyocyanin (1 hour) to the positive controls. Afterwards, levels of fluorescence were read with a microplate reader (BMG Labtech) at Ex=488nm and Em=520nm. Values were expressed as relative fluorescence units after subtracting the background fluorescence of blanks. Finally, to measure mitochondrial membrane potential ($\Delta\psi_m$), we used a mitochondrial potential detection kit (BD MitoScreen, BD Biosciences) according to manufacturer's instructions. Labelled cells were analyzed by flow cytometry and the data were expressed as percentage of cells containing depolarized mitochondria (loss of JC-1 red fluorescence).

5.8 Flow cytometry

CXCR4 membrane expression was determined by Fluorescence-activated cell sorting (FACS Calibur, BD). Cells were washed with PBS 0.5 % BSA and incubated either with PE-Cy5 mouse anti-CXCR4 monoclonal antibody (BD Biosciences) or PE-Cy5 Mouse IgG2a isotype (BD Biosciences) as control. Results of fluorescence emission were analyzed with software Cell Quest Pro and expressed as the ratio between the mean fluorescence intensity of each sample and the isotype values.

5.9 Electron microscopy

The ultrastructure of soluble (in form of nanoparticles) and insoluble (in form of IBs) T22-mRTA-H6 was observed by field emission scanning electron microscopy (FESEM). Insoluble protein was resuspended in PBS and sonicated at 10% amplitude 0.5 s ON/OFF for 1 min. Drops of 10 µL of either soluble protein in storage buffer or insoluble protein in PBS were deposited during 1 min on silicon wafers (Ted Pella), excess of liquid eliminated, and air dried. Samples without coating were observed with an in-lens detector in a FESEM Zeiss Merlin (Zeiss) operating at 1kV. Representative images were obtained at a wide range of magnifications (from 100,000x to 450,000x).

5.10 Antineoplastic effect in a disseminated acute myeloid leukemia (AML) mouse model

NSG (NOD-scid IL2R γ manull) female mice (5 weeks old) were obtained from Charles River Laboratories (Wilmington, MA, USA) and housed in microisolator units with sterile food and water *ad libitum*. After 1 week in quarantine, NSG mice were intravenously (IV) injected with luciferase-transfected THP1 cells (THP1-Luci; 1×10^6 cells/ 200 μ L) and divided randomly into three different experimental groups. One group (VEHICLE; n=3) was IV injected with NaCO₃H pH=8 buffer, a second group (T22mRTA; n=1) was administered with 10 μ g of T22-mRTA-H6. Both groups were injected with a daily dose for a total of 10 doses. A third group (IB-T22mRTA; n=2) was subcutaneously (SC) injected once with 1 mg of T22-mRTA-H6 IBs. These treatments started 2 days after the IV injection of THP1-Luci cells in mice, which generated the disseminated AML model. Evolution of AML dissemination was monitored in IVIS Spectrum three times per week until the day of the euthanasia. Weight of the animals was measured the same day of BLI analysis. All mice were euthanized the day that the first of them presented relevant signs of disease such as 10% weight loss or lack of mobility. Animals were intraperitoneally injected with luciferin, and after 5 min mice were killed by cervical dislocation. Tissues were excised and the BLI levels of the organs *ex vivo* analyzed. After that, they were preserved in formaldehyde 3.7% and paraffin embedded for further immunohistochemistry analyses. The analysis and detection of BLI was performed using radiance photons in Living Image 4.4 Software both in *in vivo* and *ex vivo* studies. All procedures were conducted in accordance with the guidelines approved by the institutional animal Ethics Committee of Hospital Sant Pau.

5.11 Histopathology and immunohistochemical staining

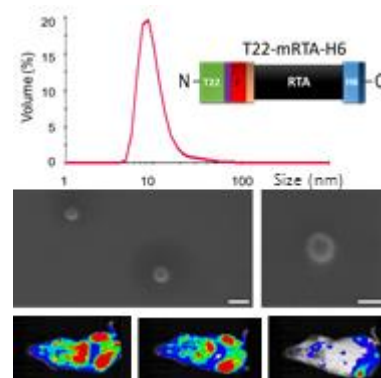
Sections of paraffin-embedded samples of infiltrated (liver, spleen, hindlimbs and backbone) and normal (lung, heart and kidney) organs were hematoxylin and eosin (H&E) stained and the presence of toxicity was analyzed. Moreover, in order to detect AML cells in infiltrated tissues, immunohistochemical analysis with anti-human CD45 antibody (DAKO) was done in paraffin-embedded tissue samples. Staining was performed in a Dako Autostainer Link 48, following the manufacturer's instructions. Two independent observers evaluated all samples, using an Olympus BX51 microscope (Olympus). Images were acquired using an Olympus DP72 digital camera and processed with CellD Imaging 3.3 software (Olympus).

5.12 Statistical analysis

Quantitative data are expressed as mean \pm standard error (SE). Previously to perform statistical analyses, all variables were tested for normality and homogeneity of variances employing the Shapiro-Wilk and the Levene test, respectively. Comparisons of soluble protein cytotoxicity effects and competition assays were made with Tukey's test. Meanwhile protein cytotoxicity assays were assessed by Mann-Whitney U tests. Significance was accepted at $p < 0.05$.

Acknowledgments. We are indebted to Agencia Estatal de Investigación (AEI) and to Fondo Europeo de Desarrollo Regional (FEDER) (grant BIO2016-76063-R, AEI/FEDER, UE), AGAUR (2017SGR-229) and CIBER-BBN (project VENOM4CANCER) granted to AV. We are also indebted to the Networking Research Center on Bioengineering, Biomaterials and Nanomedicine (CIBER-BBN) that is an initiative funded by the VI National R&D&I Plan 2008–2011, Iniciativa Ingenio 2010, Consolider Program, CIBER Actions and financed by the Instituto de Salud Carlos III, with assistance from the European Regional Development Fund. Protein production has been partially performed by the ICTS “NANBIOSIS”, more specifically by the Protein Production Platform of CIBER-BBN/ IBB (<http://www.nanbiosis.es/unit/u1-protein-production-platform-ppp/>) and the nanoparticle size analysis by the Biomaterial Processing and Nanostructuring Unit. We are also indebted to SCAC (UAB) for cell culture facilities and assistance. RD received an overseas predoctoral fellowship from Conacyt (Gobierno de México, 2016). LSG and AF were supported by AGAUR (2017FI_B100063 and 2017FI_B00680), NS by a predoctoral fellowship from the Government of Navarra, VP received a postdoctoral fellowship from the Spanish Foundation of Hematology and Hemotherapy (FEHH) and UU a Sara Borrell postdoctoral fellowship from ISCIII. AV holds an ICREA ACADEMIA award.

Received: ((will be filled in by the editorial staff))
 Revised: ((will be filled in by the editorial staff))
 Published online: ((will be filled in by the editorial staff))



The table of contents entry.

One of the most potent protein toxins in nature, ricin, has been genetically instructed to self-assemble as 11 nm-homomeric nanoparticles, that selectively kill CXCR4-overexpressing cells. These materials show a potent antitumoral effect when administered to an animal model of the difficult-to-treat disseminated acute myeloid leukemia, in complete absence of side-toxicity.

Keyword: Protein engineering, self-assembling, nanoparticles, acute myeloid leukemia, targeted drug delivery

Raquel Díaz^{1, 2, 3 §}, Dr Victor Pallarès^{4 §}, Dr Olivia Cano-Garrido^{1, 2, 3}, Naroa Serna^{1, 2, 3}, Laura Sánchez-García^{1, 2, 3}, Aïda Falgàs^{3, 4}, Dr Mireia Pesarrodona^{1, 2, 3}, Dr Ugutz Unzueta^{3, 4}, Dr Alejandro Sánchez-Chardi⁵, Dr Julieta M. Sánchez^{1, 6}, Dr Isolda Casanova^{3, 4 *}, Dr Esther Vázquez^{1, 2, 3}, Prof Ramón Mangués^{3, 4}, Prof Antonio Villaverde^{1, 2, 3 *}

¹ Institut de Biotecnologia i de Biomedicina, Universitat Autònoma de Barcelona, Bellaterra, 08193 Barcelona, Spain

² Departament de Genètica i de Microbiologia, Universitat Autònoma de Barcelona, Bellaterra, 08193 Barcelona, Spain

³ CIBER de Bioingeniería, Biomateriales y Nanomedicina (CIBER-BBN), Bellaterra, 08193 Barcelona, Spain

⁴ Biomedical Research Institute Sant Pau (IIB-Sant Pau) and Josep Carreras Research Institute, Hospital de la Santa Creu i Sant Pau, 08025 Barcelona, Spain

⁵ Servei de Microscòpia, Universitat Autònoma de Barcelona, Bellaterra, 08193 Barcelona, Spain

⁶ Instituto de Investigaciones Biológicas y Tecnológicas (IIBYT) (CONICET-Universidad Nacional de Córdoba). ICTA & Cátedra de Química Biológica, Departamento de Química, FCEFYN, UNC. Av. Velez Sarsfield 1611, X 5016GCA Córdoba, Argentina

Title Selective CXCR4+ cancer cell targeting and potent antineoplastic effect by a nanostructured version of recombinant ricin

References

1. Siegel, R. L.; Miller, K. D.; Jemal, A., *CA: a cancer journal for clinicians* **2018**, *68* (1), 7.
2. Vincenzi, B.; Armento, G.; Spalato Ceruso, M.; Catania, G.; Lealos, M.; Santini, D.; Minotti, G.; Tonini, G., *Expert opinion on drug safety* **2016**, *15* (9), 1219.
3. Serna, N.; Sanchez-Garcia, L.; Unzueta, U.; Diaz, R.; Vazquez, E.; Mangués, R.; Villaverde, A., *Trends in biotechnology* **2017**. DOI 10.1016/j.tibtech.2017.11.007.
4. Shen, J.; Wolfram, J.; Ferrari, M.; Shen, H., *Materials today* **2017**, *20* (3), 9.
5. Sanchez-Garcia, L.; Martin, L.; Mangués, R.; Ferrer-Miralles, N.; Vazquez, E.; Villaverde, A., *Microbial cell factories* **2016**, *15*, 33.
6. Kintzing, J. R.; Filsinger Interrante, M. V.; Cochran, J. R., *Trends in pharmacological sciences* **2016**, *37* (12), 993.
7. Manoukian, G.; Hagemester, F., *Expert opinion on biological therapy* **2009**, *9* (11), 1445.
8. Hassan, R.; Sharon, E.; Thomas, A.; Zhang, J.; Ling, A.; Miettinen, M.; Kreitman, R. J.; Steinberg, S. M.; Hollevoet, K.; Pastan, I., *Cancer* **2014**, *120* (21), 3311.
9. Kreitman, R. J.; Pastan, I., *Best practice & research. Clinical haematology* **2015**, *28* (4), 236.
10. Polito, L.; Djemil, A.; Bortolotti, M., *Biomedicines* **2016**, *4* (2). DOI 10.3390/biomedicines4020012.
11. Wittstock, U.; Gershenzon, J., *Current opinion in plant biology* **2002**, *5* (4), 300.

12. Cummings, R. D.; R, L. S., R-Type Lectins. In *Essentials of Glycobiology*, rd; Varki, A.; Cummings, R. D.; Esko, J. D.; Stanley, P.; Hart, G. W.; Aebi, M.; Darvill, A. G.; Kinoshita, T.; Packer, N. H.; Prestegard, J. H.; Schnaar, R. L.; Seeberger, P. H., Eds. Cold Spring Harbor (NY), 2015; pp 401-412.
13. Moshiri, M.; Hamid, F.; Etemad, L., *Reports of biochemistry & molecular biology* **2016**, 4 (2), 60.
14. Kulbe, H.; Levinson, N. R.; Balkwill, F.; Wilson, J. L., *The International journal of developmental biology* **2004**, 48 (5-6), 489.
15. Murakami, T.; Cardones, A. R.; Hwang, S. T., *Journal of dermatological science* **2004**, 36 (2),.
16. Balkwill, F., *Seminars in cancer biology* **2004**, 14 (3), 171.
17. Kim, J.; Takeuchi, H.; Lam, S. T.; Turner, R. R.; Wang, H. J.; Kuo, C.; Foshag, L.; Bilchik, A. J.; Hoon, D. S., *J Clin Oncol* **2005**, 23 (12), 2744.
18. Burger, J. A.; Kipps, T. J., *Blood* **2006**, 107 (5), 1761.
19. Kim, J.; Mori, T.; Chen, S. L.; Amersi, F. F.; Martinez, S. R.; Kuo, C.; Turner, R. R.; Ye, X.; Bilchik, A. J.; Morton, D. L.; Hoon, D. S., *Annals of surgery* **2006**, 244 (1), 113.
20. Unzueta, U.; Cespedes, M. V.; Ferrer-Miralles, N.; Casanova, I.; Cedano, J.; Corchero, J. L.; Domingo-Espin, J.; Villaverde, A.; Mangués, R.; Vázquez, E., *International journal of nanomedicine* **2012**, 7, 4533.
21. Cespedes, M. V.; Unzueta, U.; Alamo, P.; Gallardo, A.; Sala, R.; Casanova, I.; Pavon, M. A.; Mangués, M. A.; Trias, M.; Lopez-Pousa, A.; Villaverde, A.; Vázquez, E.; Mangués, R., *Nanomedicine : nanotechnology, biology, and medicine* **2016**, 12 (7), 1987.
22. Serna, N. C., M; Sánchez-García, L; Unzueta, U; Sala, R; Sánchez-Chardi, A; Cortés, F; Ferrer-Miralles, N; Mangués, R; Vázquez, E; Villaverde, A, *Advanced Functional Materials* **2017**, 27, 1700919..

23. Sanchez-Garcia, L.; Serna, N.; Alamo, P.; Sala, R.; Cespedes, M. V.; Roldan, M.; Sanchez-Chardi, A.; Unzueta, U.; Casanova, I.; Mangués, R.; Vazquez, E.; Villaverde, A., *Journal of controlled release : official journal of the Controlled Release Society* **2018**. DOI 10.1016/j.jconrel.2018.01.031.
24. Gonzalez-Montalban, N.; Garcia-Fruitos, E.; Villaverde, A., *Nature biotechnology* **2007**, *25* (7), 718.
25. Cespedes, M. V.; Fernandez, Y.; Unzueta, U.; Mendoza, R.; Seras-Franzoso, J.; Sanchez-Chardi, A.; Alamo, P.; Toledo-Rubio, V.; Ferrer-Miralles, N.; Vazquez, E.; Schwartz, S.; Abasolo, I.; Corchero, J. L.; Mangués, R.; Villaverde, A., *Scientific reports* **2016**, *6*, 35765.
26. Seras-Franzoso, J.; Sanchez-Chardi, A.; Garcia-Fruitos, E.; Vazquez, E.; Villaverde, A., *Soft matter* **2016**, *12* (14), 3451.
27. Unzueta, U.; Seras-Franzoso, J.; Cespedes, M. V.; Saccardo, P.; Cortes, F.; Rueda, F.; Garcia-Fruitos, E.; Ferrer-Miralles, N.; Mangués, R.; Vazquez, E.; Villaverde, A., *Nanotechnology* **2017**, *28* (1), 015102..
28. Unzueta, U.; Ferrer-Miralles, N.; Cedano, J.; Zikung, X.; Pesarrodona, M.; Saccardo, P.; Garcia-Fruitos, E.; Domingo-Espin, J.; Kumar, P.; Gupta, K. C.; Mangués, R.; Villaverde, A.; Vazquez, E., *Biomaterials* **2012**, *33* (33), 8714.
29. Pesarrodona, M.; Crosas, E.; Cubarsi, R.; Sanchez-Chardi, A.; Saccardo, P.; Unzueta, U.; Rueda, F.; Sanchez-Garcia, L.; Serna, N.; Mangués, R.; Ferrer-Miralles, N.; Vazquez, E.; Villaverde, A., *Nanoscale* **2017**, *9* (19), 6427.
30. Rueda, F.; Cespedes, M. V.; Conchillo-Sole, O.; Sanchez-Chardi, A.; Seras-Franzoso, J.; Cubarsi, R.; Gallardo, A.; Pesarrodona, M.; Ferrer-Miralles, N.; Daura, X.; Vazquez, E.; Garcia-Fruitos, E.; Mangués, R.; Unzueta, U.; Villaverde, A., *Advanced materials* **2015**, *27* (47), 7816.
31. Webb, B. A.; Chimenti, M.; Jacobson, M. P.; Barber, D. L., *Nature reviews. Cancer* **2011**, *11* (9), 671.

32. Corbet, C.; Feron, O., *Nature reviews. Cancer* **2017**, *17* (10), 577.
33. Jung, Y. H.; Lee, D. Y.; Cha, W.; Kim, B. H.; Sung, M. W.; Kim, K. H.; Ahn, S. H., *Head & neck* **2016**, *38* (10), 1479.
34. Momparler, R. L., *Experimental hematology & oncology* **2013**, *2*, 20.
35. Richard, J. P.; Melikov, K.; Vives, E.; Ramos, C.; Verbeure, B.; Gait, M. J.; Chernomordik, L. V.; Lebleu, B., *The Journal of biological chemistry* **2003**, *278* (1), 585.
36. Pesarrodonna, M.; Fernandez, Y.; Foradada, L.; Sanchez-Chardi, A.; Conchillo-Sole, O.; Unzueta, U.; Xu, Z.; Roldan, M.; Villegas, S.; Ferrer-Miralles, N.; Schwartz, S., Jr.; Rinas, U.; Daura, X.; Abasolo, I.; Vazquez, E.; Villaverde, A., *Biofabrication* **2016**, *8* (2), 025001..
37. Vazquez, E.; Mangués, R.; Villaverde, A., *Nanomedicine* **2016**, *11* (11), 1333.
38. Tomlinson, I. M., *Nature biotechnology* **2004**, *22* (5), 521.
39. Agyei, D.; Ahmed, I.; Akram, Z.; Iqbal, H. M.; Danquah, M. K., *Protein and peptide letters* **2017**, *24* (2), 94.
40. Aruna, G., *Journal of stem cells & regenerative medicine* **2006**, *1* (1), 31.
41. Alewine, C.; Hassan, R.; Pastan, I., *The oncologist* **2015**, *20* (2), 176.
42. Akbari, B.; Farajnia, S.; Ahdi Khosroshahi, S.; Safari, F.; Yousefi, M.; Dariushnejad, H.; Rahbarnia, L., *International reviews of immunology* **2017**, *1*.
43. Duncan, R.; Gaspar, R., *Molecular pharmaceuticals* **2011**, *8* (6), 2101.
44. Stefan Wilhelm, A. J. T., Qin Dai, Seiichi Ohta, Julie Audet, Harold F. Dvorak & Warren C. W. Chan, *Nature Reviews Materials* **2016**, *1*.
45. Unzueta, U.; Cespedes, M. V.; Vazquez, E.; Ferrer-Miralles, N.; Mangués, R.; Villaverde, A., *Trends in biotechnology* **2015**, *33* (5), 253.
46. Tyagi, N.; Tyagi, M.; Pachauri, M.; Ghosh, P. C., *Tumour biology : the journal of the International Society for Oncodevelopmental Biology and Medicine* **2015**, *36* (11), 8239.

47. Bellisola, G.; Fracasso, G.; Ippoliti, R.; Menestrina, G.; Rosen, A.; Solda, S.; Udali, S.; Tomazzolli, R.; Tridente, G.; Colombatti, M., *Biochemical pharmacology* **2004**, *67* (9), 1721.
48. Schnell, R.; Borchmann, P.; Staak, J. O.; Schindler, J.; Ghetie, V.; Vitetta, E. S.; Engert, A., *Ann Oncol* **2003**, *14* (5), 729.
49. Lambert, J. M.; Goldmacher, V. S.; Collinson, A. R.; Nadler, L. M.; Blattler, W. A., *Cancer research* **1991**, *51* (23 Pt 1), 6236.
50. Gottesman, M. M.; Fojo, T.; Bates, S. E., *Nature reviews. Cancer* **2002**, *2* (1), 48.
51. Kapse-Mistry, S.; Govender, T.; Srivastava, R.; Yergeri, M., *Frontiers in pharmacology* **2014**, *5*, 159.
52. Kirtane, A. R.; Kalscheuer, S. M.; Panyam, J., *Advanced drug delivery reviews* **2013**, *65* (13-14), 1731.
53. Wales, R.; Roberts, L. M.; Lord, J. M., *The Journal of biological chemistry* **1993**, *268* (32), 23986.
54. Vallera, D. A.; Chen, H.; Sicheneder, A. R.; Panoskaltsis-Mortari, A.; Taras, E. P., *Leuk Res* **2009**, *33* (9), 1233.
55. Yamada, Y.; Aoyama, A.; Tocco, G.; Boskovic, S.; Nadazdin, O.; Alessandrini, A.; Madsen, J. C.; Cosimi, A. B.; Benichou, G.; Kawai, T., *Journal of immunology* **2012**, *188* (12), 6063.
56. Murphy, J. R.; vanderSpek, J. C., *Seminars in cancer biology* **1995**, *6* (5), 259.
57. Onda, M.; Willingham, M.; Wang, Q. C.; Kreitman, R. J.; Tsutsumi, Y.; Nagata, S.; Pastan, I., *Journal of immunology* **2000**, *165* (12), 7150.
58. Newton, D. L.; Nicholls, P. J.; Rybak, S. M.; Youle, R. J., *The Journal of biological chemistry* **1994**, *269* (43), 26739.
59. Porter, S., *Journal of pharmaceutical sciences* **2001**, *90* (1), 1.

60. Grinberg, Y.; Benhar, I., *Biomedicines* **2017**, *5* (2). DOI 10.3390/biomedicines5020028.
61. Wang, Y.; Xie, Y.; Oupicky, D., *Current pharmacology reports* **2016**, *2* (1), 1.
62. Heckmann, D.; Maier, P.; Laufs, S.; Wenz, F.; Zeller, W. J.; Fruehauf, S.; Allgayer, H., *Translational oncology* **2013**, *6* (2), 124.
63. Choi, W. T.; Yang, Y.; Xu, Y.; An, J., *Current topics in medicinal chemistry* **2014**, *14* (13), 1574.
64. Philipp-Abbrederis, K.; Herrmann, K.; Knop, S.; Schottelius, M.; Eiber, M.; Luckerath, K.; Pietschmann, E.; Habringer, S.; Gerngross, C.; Franke, K.; Rudelius, M.; Schirbel, A.; Lapa, C.; Schwamborn, K.; Steidle, S.; Hartmann, E.; Rosenwald, A.; Kropf, S.; Beer, A. J.; Peschel, C.; Einsele, H.; Buck, A. K.; Schwaiger, M.; Gotze, K.; Wester, H. J.; Keller, U., *EMBO molecular medicine* **2015**, *7* (4), 477.
65. Goranova, T. E.; Bozhanov, S. S.; Lozanov, V. S.; Mitev, V. I.; Kaneva, R. P.; Georgieva, E. I., *Neoplasma* **2015**, *62* (1), 27.
66. Tamas, K.; Domanska, U. M.; van Dijk, T. H.; Timmer-Bosscha, H.; Havenga, K.; Karrenbeld, A.; Sluiter, W. J.; Beukema, J. C.; van Vugt, M. A.; de Vries, E. G.; Hospers, G. A.; Walenkamp, A. M., *Current pharmaceutical design* **2015**, *21* (17), 2276.
67. Li, M. Y.; Bruzzone, R.; Wang, P. G., *Oncotarget* **2015**, *6* (31), 30425.